

pubs.acs.org/biochemistry Article

Impact of N-Glycosylation on Protein Structure and Dynamics Linked to Enzymatic C-H Activation in the M. oryzae Lipoxygenase

Chris Whittington, Ajay Sharma, S. Gage Hill, Anthony T. Iavarone, Brian M. Hoffman, and Adam R. Offenbacher*



Cite This: Biochemistry 2024, 63, 1335-1346



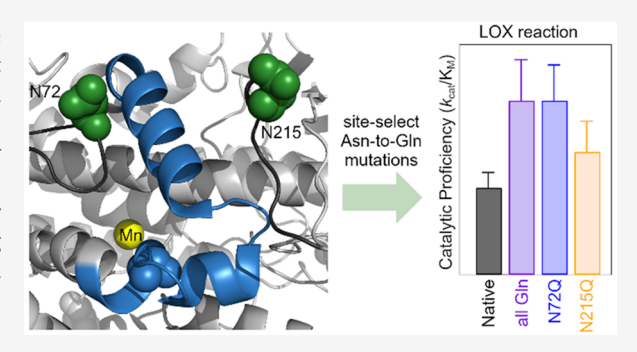
ACCESS I

III Metrics & More

Article Recommendations

s Supporting Information

ABSTRACT: Lipoxygenases (LOXs) from pathogenic fungi are potential therapeutic targets for defense against plant and select human diseases. In contrast to the canonical LOXs in plants and animals, fungal LOXs are unique in having appended *N*-linked glycans. Such important post-translational modifications (PTMs) endow proteins with altered structure, stability, and/or function. In this study, we present the structural and functional outcomes of removing or altering these surface carbohydrates on the LOX from the devastating rice blast fungus, *M. oryzae*, *Mo*LOX. Alteration of the PTMs did notinfluence the active site enzyme—substrate ground state structures as visualized by electron—nuclear double resonance (ENDOR) spectroscopy. However, removal of the eight *N*-linked glycans by asparagine-to-



glutamine mutagenesis nonetheless led to a change in substrate selectivity and an elevated activation energy for the reaction with substrate linoleic acid, as determined by kinetic measurements. Comparative hydrogen—deuterium exchange mass spectrometry (HDX-MS) analysis of wild-type and Asn-to-Gln MoLOX variants revealed a regionally defined impact on the dynamics of the arched helix that covers the active site. Guided by these HDX results, a single glycan sequon knockout was generated at position 72, and its comparative substrate selectivity from kinetics nearly matched that of the Asn-to-Gln variant. The cumulative data from model glyco-enzyme MoLOX showcase how the presence, alteration, or removal of even a single N-linked glycan can influence the structural integrity and dynamics of the protein that are linked to an enzyme's catalytic proficiency, while indicating that extensive glycosylation protects the enzyme during pathogenesis by protecting it from protease degradation.

ipoxygenases (LOXs) are widely distributed in plants, animals, and pathogenic fungi. The canonical LOXs, found in plants and animals, oxidize polyunsaturated fatty acids to form an extensive collection of potent and bioactive cell signaling mediators for the host organism. Plant and animal LOXs consist of two domains, a primarily α helical catalytic domain and an N-terminal, C2-like polycystin-1/LOX/ α -toxin (PLAT) domain, which mediates membrane association and can regulate LOX function.^{2,3} The LOX gene in fungi lack this N-terminal domain, but contain a secretion signal.⁴⁻⁷ With this signal peptide, fungal pathogens secrete LOXs during invasion, and the enzymes contribute to pathogenesis through the oxidation of lipids in plants and animals. 6,8 The LOXs from pathogenic fungi are unique, as they are the only known class of LOXs with heterogeneous, N-linked glycosylation, which differentiates them from the canonical homologs of plants and animals, which lack such post-translational modifications (PTMs).^{6,9,10}

Glycan PTMs are an important structural feature of many macromolecules and are responsible for the regulation of a broad spectrum of cellular functions. Diverse biological macromolecules exhibit glycosylation, including proteins (glycoproteins and proteoglycans), lipids (glycolipids), and

more recently, ¹² RNA. For proteins, glycans can be *N*- or *O*-linked, with *N*-linked glycans covalently bound to asparagine within the defined three amino acid sequon, Asn-X-(Thr/Ser). They facilitate protein folding, protein trafficking for secretion, and/or membrane presentation. ^{13,14} Glycans also have been shown to help stabilize protein structure and to protect against proteolysis. ¹⁵ Mis- or altered glycosylation has been associated with over 125 disease states in humans, including the congenital disorders rheumatoid arthritis and diabetes, presumably functioning through altered cellular recognition and/or changes to the protein structure and stability. ^{16–19} One of the inherent challenges in studying glycoproteins is the difficulty in characterizing their structure by conventional X-ray diffraction methods, as the branched and dynamic nature of

Received: February 28, 2024
Revised: April 18, 2024
Accepted: April 23, 2024
Published: May 1, 2024





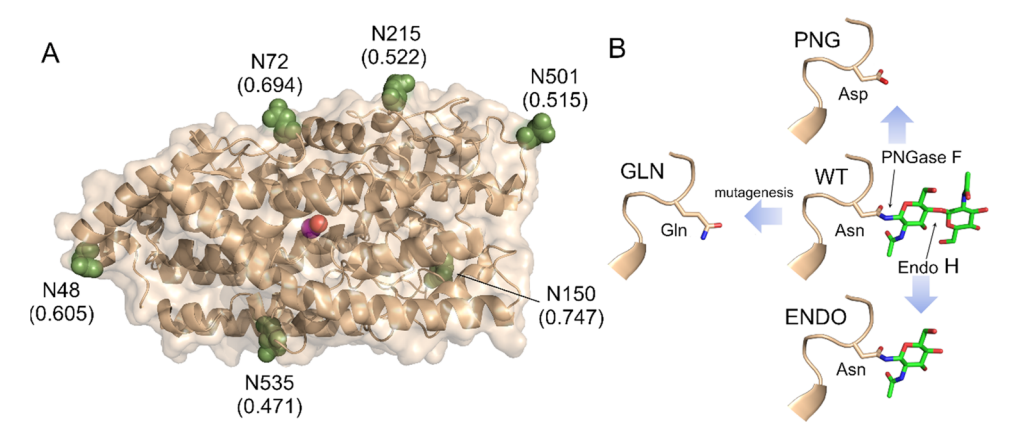


Figure 1. X-ray crystal structure of MoLOX with the Asn residues forming putative N-linked glycosylation sites shown as spheres (A). The potential for N-linked glycosylation sites is listed in parentheses. The catalytic cofactor, Mn^{2+} – OH_2 , is represented as purple and red spheres, respectively. (B) Diagram illustrating the methods for N-linked glycan processing (blue arrows). The green sticks represent N-acetylglucosamine (N-GlcNAc) residues, and the full glycan structures have been removed for clarity. For "GLN" MoLOX variant, all eight asparagine residues that are predicted N-linked glycosylation sites were mutated to glutamine.

Scheme 1. Mechanism of Substrate Oxidation by MoLOX

the (sometimes heterogeneous) carbohydrate assemblies can inhibit crystallization. ²⁰

The lipoxygenase MoLOX is produced by one of the most devastating fungal pathogens, Magnaporthe oryzae, which causes rice blast disease; this plant pathogen is responsible for the loss of nearly one-third of the world's rice crop.²¹ MoLOX has been cloned and recombinantly expressed in the yeast P. pastoris, enabling high protein yields for biochemical and structural studies of the glycosylated protein.⁶ For example, a crystal structure was solved for MoLOX, in which the N-linked glycans were removed by endonuclease H (Endo H), providing a topographical map of the protein (Figure 1A).²² This structure did not contain substrate and thus lacked detailed information about how the substrate binds in the active site. While modification or removal of glycans can enable crystal formation for high-resolution protein structural analysis, there are several examples where removal of carbohydrates from an enzyme surface leads to altered catalytic proficiency. 23,24 Thus, an understanding of how glycosylation influences protein structure, dynamics, and function is of considerable importance.

Structural insight into the costructure of the native, glycosylated *Mo*LOX with substrate linoleic acid, LA, was recently achieved with electron—nuclear double resonance (ENDOR) spectroscopy, which identified the orientation and positioning of the substrate with respect to the paramagnetic

metal center manganese (Mn²⁺) at the active site.²⁵ ENDOR analysis also revealed that the positioning of LA in the *Mo*LOX active site remains unchanged after alteration of the glycan structure using Endo H. This approach thus can overcome the inability to acquire X-ray structural information for the native, fully glycosylated form of *Mo*LOX.

Glycosidase treatment of MoLOX was previously shown to impact catalysis, as revealed by changes in catalytic kinetic parameters, ^{25,26} but this was not accompanied by a comprehensive biophysical study exploring the effects of systematic alteration of glycosylation patterns on the structure-function relationships of fungal LOXs. In the current study, the kinetic and structural consequences of removal of the N-linked glycans from MoLOX are explored for a series of protein variants with altered or eliminated glycans (Figure 1B). Deglycosylation of WT MoLOX is performed either by treatment with the glycosylases, peptide:N-glycosidase F (PNGase F), Endo H, or through mutagenesis. For the latter, the eight Asn residues, which were predicted by NeNGlyc server²⁷ to be linked to a carbohydrate, were all mutated to glutamine (GLN MoLOX variant; Figure 1B). The impact of the PTMs on protein structural stability was determined by limited proteolysis experiments. Kinetic isotope effects were used to probe how glycosylation might alter the multidimensional barriers of the MoLOX reaction with LA that is initiated by a rate-limiting hydrogen transfer process

(Scheme 1).²⁶ The influence of glycosylation on the substrate positioning in the active site was examined by ENDOR spectroscopy.

We also extended the kinetic analysis to other substrates. The MoLOX oxidation kinetics were assessed for α -linolenic (αLA) , γ -linolenic (γLA) , and arachidonic acid (AA), and the Michaelis-Menten rate constants were compared to those of LA. Hydrogen-deuterium exchange mass spectrometry (HDX-MS) experiments were utilized to reveal the regional differences in the protein structure and flexibility across the different MoLOX glycan forms. Based on these results, we have found which of the eight glycans in wild-type enzyme have the greatest impact on the kinetic and HDX properties. Siteselective mutations were generated at these sites (i.e., N72Q and N215Q), and the reaction kinetics were determined for the four substrates of LA, α LA, γ LA, and AA. The cumulative kinetic and HDX data suggest that a single glycan, located more than 20 Å from the active site, can tune the catalytic proficiency of the enzyme as mediated through dynamic alteration of regional peptide flexibility.

METHODS

Materials. LA, γ LA, α LA, and AA were purchased from Acros Organic, TCI (Palo Alto, CA), and Cayman Chemical Company (Ann Arbor, MI), respectively. Deuterium oxide (D₂O, 99% D), NaOD (99% D), and DCl (99% D) were purchased from Cambridge Isotopes (Tewksbury, MA). Dideuterated linoleic acid (11,11-D₂-LA) was synthesized previously. All yeast/bacterial cells, media, salts, and buffers were purchased from Fisher Scientific, Sigma-Aldrich, or VWR at the highest grade possible.

MoLOX Expression and Purification. Wild-type (WT) MoLOX was expressed in and purified from P. pastoris X-33 cells as previously described. The "GLN" mutant was generated from the mutagenesis of eight asparagine residues forming predicted glycan sites (N18, N28, N48, N72, N150, N215, N501, and N535) to glutamine. This gene was generated by GenScript (Piscataway, NJ). GLN MoLOX purification required the use of a butyl sepharose column for the initial capture via hydrophobic interaction chromatography (HIC). The final purification for all variants was carried out using a HiPrep 26/60 Sephacryl S-200 column on an AKTA FPLC system with 50 mM HEPES (pH 7.5), 150 mM NaCl, and 10% glycerol. The fractions that corresponded to the peak with lipoxygenase activity were concentrated to 100 μ M, frozen in aliquots with $N_2(1)$, and stored at -80 °C. Mn content was determined using ICP-OES. ENDO MoLOX was prepared by treating WT MoLOX with EndoH in a 20:1 (MoLOX:EndoH) mass ratio and further purified as described previously.²⁵ PNG MoLOX was prepared using PNGase F Prime from Bulldog Bio using our previously published protocol.20

Enzyme Kinetics. *Mo*LOX enzyme kinetics were measured using a Hansatech oxygen (O_2) electrode. LA, dideuterated LA (11,11- D_2 -LA), α LA, γ LA, and AA concentrations were determined enzymatically, as previously described, using soybean lipoxygenase as isolated from bacterial cultures. Kinetic parameters ($k_{\rm cat}$ and $k_{\rm cat}/K_{\rm M}$) were extracted from nonlinear fits to the Michaelis–Menten equation. Kinetic assays for pH dependence were performed at 20 °C in 0.1 M Tris-HCl (pH 7) or 0.1 M borate (pH 9) with substrate concentrations from 2 to 100 μ M. For temperature-dependent studies, kinetic assays were performed at 10, 12.5, 15, 20, 25,

27.5, and 30 °C and in 0.1 M borate (pH 9) with substrate concentrations ranging from 2 to 100 μ M. The lower concentrations of LA for pH dependence were necessary to keep it below the critical micelle concentrations, which are reduced at lower pH values.

Circular Dichroism (CD) Spectroscopy. Structure was assessed by CD using a Jasco model J-815 CD spectrometer at room temperature with bandwidths of 2 nm with a Starna cell (path length of 0.1 cm). Samples were recorded at 25 °C in 25 mM potassium phosphate (pH 7). The concentrations were adjusted so that the photomultiplier tube high voltage remained \leq 600 V in the range of 190–260 nm. Measurements for stability were also carried out with wavelengths set to 222 nm and the temperature range of 25–90 °C (2 °C intervals) with a temperature ramp up rate of 0.6 °C/min.

ENDOR Spectroscopy. Q-band echo-detected electron paramagnetic resonance (EPR) spectra (two-pulse echo sequence, $\pi/2-\tau-\pi-\tau$ -echo) and Davies/Mims pulsed ENDOR spectra were collected on a spectrometer that has been described. All measurements were done with a helium immersion dewar, at 2 K. The Mims pulsed ENDOR sequence (three-pulse echo sequence, $\pi/2-\tau-\pi/2-T-\pi/2-\tau$ -echo, with radio frequency (rf) pulse ($T_{\rm rf}$) inserted in the interval, T, between second and third pulses) was used to probe the $^{13}{\rm C}$ hyperfine coupling of $^{13}{\rm C}10$, $^{13}{\rm C}11$ nuclei of labeled LA substrate. Previous EPR and ENDOR simulations, performed on the WT MoLOX, are reported elsewhere.

Hydrogen–Deuterium Exchange Mass Spectrometry (HDX-MS). Peptides from the pepsin-digested WT MoLOX were previously assigned using LC–tandem MS (MS/MS). Using these peptides, HDX measurements were carried out through 10-fold dilution of MoLOX (WT, ENDO, GLN, and PNG) in 50 mM HEPES (pD 7.5), 150 mM NaCl D₂O buffer. Samples were incubated on a water bath at 20 °C. At a specified time, a sample was cold and acid quenched (to pH 2.4) to minimize back-exchange. The samples were digested with immobilized pepsin for 2.5 min. Prior to digestion, guanidine HCl (pH 2.4) was added to a final concentration of 0.5 M. The pepsin was removed by filtration and the samples were flash frozen in liquid N₂ and stored at -80 °C until data collection.

Deuterated, pepsin-digested samples of *Mo*LOX from HDX experiments were analyzed using a 1200 series liquid chromatography (LC) system (Agilent, Santa Clara, CA) that was connected in-line with an LTQ-Orbitrap-XL mass spectrometer (Thermo Fisher Scientific, Waltham, MA). Instrument and sample collection details are described elsewhere. Data acquisition was controlled using Xcalibur software (version 2.0.7, Thermo). Mass spectral data acquired for HDX measurements were analyzed using the software, HDX WorkBench. The percent deuterium incorporation for each peptide has been normalized for 100% D₂O and corrected for peptide-specific back-exchange, as previously described.

RESULTS

Sample Preparation. *Mo*LOX was isolated from yeast cultures as previously described with typical yields of 10–15 mg per liter of culture. This sample was used to prepare the PNGaseF- (denoted PNG) and EndoH-treated (denoted ENDO) variants of *Mo*LOX. Sodium dodecyl sulfate—polyacrylamide gel electrophoresis (SDS–PAGE) of ENDO and PNG corroborated the expected loss of mass associated with the truncation of the N-linked glycosylation (Figure S1).

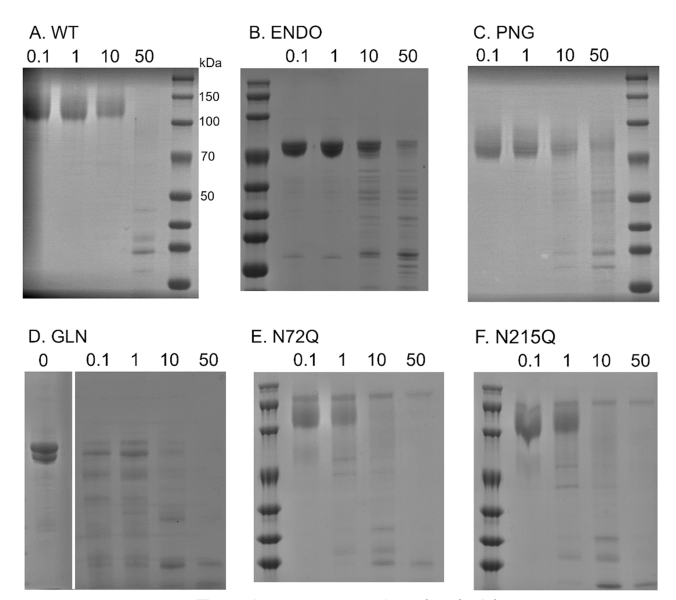
Size exclusion chromatography (SEC) further showed that the elution of the ENDO *Mo*LOX variant was ~70 kDa, consistent with a monomeric species. It is important to note that the PNGase F-treated MoLOX sample migrated differently than ENDO *Mo*LOX, suggesting that deglycosylation by PNGase F may not proceed to completion.

A variant, denoted the GLN variant, was also constructed, in which all eight Asn residues predicted to house N-linked glycans (Figure 1A) were mutated to glutamine to eliminate all carbohydrates on the protein. High-resolution mass spectrometry of the intact, WT MoLOX produced a broad MS feature indicative of protein mass heterogeneity. This MS behavior is in line with the expectation that the N-linked carbohydrates on MoLOX are heterogeneous^{6,9} and precludes detailed MS characterization of the individual glycan structures. Previous MS/MS experiments on the PNG MoLOX identified four glycan sites (N18, N28, N48, and N501) by the presence of Asp at the predicted glycan sites.²⁶ From the X-ray crystal structure of ENDO MoLOX, three N-GlcNAc residues were resolved at positions N72, N150, and N535.²² In addition to these seven N-linked glycan sites, a glycan site at N215 is also predicted.²⁷ Expression and purification of GLN-MoLOX from P. pastoris, similar to that for the native form, resulted in slightly lower protein yields at 5 mg/L. Alternative expression of MoLOX in E. coli to produce a nonglycosylated protein led to the formation of the protein in inclusion bodies.2

MoLOX Thermal and Proteolytic Stability. Secondary structural analysis of the four MoLOX variants using circular dichroism (CD) spectroscopy revealed nearly superimposable spectra, confirming that the proteins are intact and consistent with the native fold (Figure S1). Temperature-dependent CD was also used to estimate the thermostability of the MoLOX variants. The corresponding melting temperatures ($T_{\rm m}$) from this analysis are presented in Table S1. The $T_{\rm m}$ of WT MoLOX was 59.8 ± 0.2 °C, with slight decreases in the stability ($\Delta T_{\rm m} = 5-6$ °C) observed for the ENDO and GLN variants (Table S1).

Next, the proteolytic stability of the different variants was tested by limited proteolysis experiments. Briefly, MoLOX was incubated with varying concentrations of trypsin for 1 h and the degree of protein degradation was visualized by SDS–PAGE (Figure 2). The WT enzyme showed the least susceptibility to trypsin, with minimal degradation up to 10 μ g/mL trypsin and degradation apparent at 50 μ g/mL. ENDO and PNG variants were more susceptible to trypsin with noticeable degradation starting at 10 μ g/mL trypsin. The most susceptible variant to proteolysis was the GLN variant which showed noticeable degradation even at lower concentrations of trypsin. Thus, the glycans on WT MoLOX aid in the protection against proteolytic digestion. This behavior has been noted for other secretory proteins.

Reaction of MoLOX with Linoleic Acid (LA). The impact of removing these glycans from the WT enzyme was initially examined using steady-state kinetics of the MoLOX reaction with LA, the most abundant substrate in rice. PNG MoLOX showed a ~40% increase in the first-order rate constant, $k_{\rm cat}$ paired with an unchanged second-order rate constant (enzyme proficiency, $k_{\rm cat}/K_{\rm M}$), while the $k_{\rm cat}$ value for ENDO MoLOX was unchanged from WT (Tables 1 and S2). The GLN variant exhibited a ~70% increase in $k_{\rm cat}$. However, the GLN variant is also associated with a 100% increase in the second-order rate constant: $k_{\rm cat}/K_{\rm M} = 0.34 \pm 0.08~\mu{\rm M}^{-1}~{\rm s}^{-1}$, compared to $0.17 \pm 0.03~\mu{\rm M}^{-1}~{\rm s}^{-1}$ for WT MoLOX. These kinetic properties show



Trypsin concentration (μg/mL)

Figure 2. Proteolytic stability of *Mo*LOX variants as determined by limited proteolysis and visualized by SDS-PAGE. The labels correspond to (A) WT, (B) ENDO, (C) PNG, (D) GLN, (E) N72Q, and (F) N215Q *Mo*LOX variants. Each variant was incubated with trypsin (0.1–50 μ g/mL) at 37 °C for 1 h. The buffer was 50 mM HEPES, 150 mM NaCl, pH 7.5, supplemented with 1 mM CaCl₂.

that complete removal of the glycans from the side chain (either Asp or Gln) results in increased catalytic rate and/or enzyme proficiency.

Next, we investigated the effect of the glycans on the efficiency of hydrogen tunneling associated with substrate oxidation by LOXs. The initial and rate-limiting chemical step for the oxidation of LA and other fatty acids by LOXs is an irreversible C-H cleavage step by a proton-coupled electron transfer process in which a hydrogen atom of substrate is transferred to a metal-bound hydroxide, with the electron reducing the metal (Scheme 1).35,36 The reaction of WT MoLOX with deuterated LA (11,11-2H₂) is characterized by a large isotope effect, ${}^{\rm D}k_{\rm cat}\approx 70$, which is invariant with temperature. ²⁶ These kinetic parameters are characteristic of nonclassical, hydrogen tunneling mechanism. ^{37–39} Using these kinetic values from WT MoLOX as a guidelines for tunneling efficiency, there are no significant differences in the isotope effects (${}^{\mathrm{D}}k_{\mathrm{cat}}$) or their temperature dependencies (ΔE_{a}) across the WT and deglycosylated MoLOX variants except for a subtle increase in the ΔE_a for PNG²⁶ and a slight decrease in the ${}^{\mathrm{D}}k_{\mathrm{cat}}$ for GLN. These data support that all variants exhibit deep tunneling effects for rate-limiting hydrogen transfer and that the tunneling properties are largely unchanged.

The changes in the rate constants for the GLN variant are also accompanied by an increase in the activation energy (E_a) for the reaction with unlabeled LA. The E_a values of the PNG and ENDO variants are comparable to WT MoLOX (9–10 kcal/mol), ²⁶ while the GLN variant exhibited an elevated E_a value of 12 \pm 0.7 kcal/mol. Consistent with our finding, a previous kinetic study on the tunneling enzyme glucose oxidase, GOx, revealed that alterations of the native glycans were also associated with an altered E_a for H-transfer. ⁴⁰ In the theoretical treatments of these enzymatic H-transfer reactions by tunneling, ^{35,41,42} hydrogenic wave function overlap is inherently temperature independent. The empirical temper-

Table 1. Kinetic Parameters for MoLOX Variants and Their Reactions with Substrate, LA

MoLOX variant	$k_{\rm cat}^{a} (\rm s^{-1})$	$k_{\rm cat}/K_{\rm M}^{\ \ a} \ (\mu { m M}^{-1} \ { m s}^{-1})$	$E_a(H)$ (kcal/mol)	${}^{\mathrm{D}}k_{\mathrm{cat}}{}^{a,b}$	ΔE_a^c (kcal/mol)
WT	1.65 ± 0.08	0.17 ± 0.03	9.6 ± 0.5	70 ± 2	-1 ± 0.6
PNG^d	2.33 ± 0.27	0.13 ± 0.02	9.7 ± 0.6	73 ± 3	0.6 ± 0.6
ENDO ^e	1.78 ± 0.10	0.12 ± 0.02	8.5 ± 1.0	70 ± 6	-0.9 ± 1.5
GLN	2.76 ± 0.16	0.34 ± 0.08	12.1 ± 0.7	57 ± 5	-1.1 ± 0.8

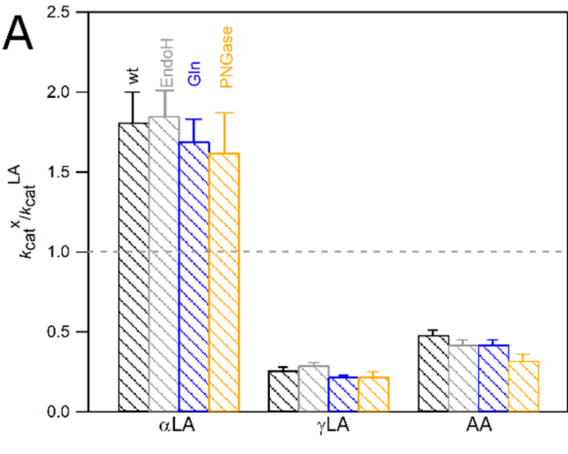
^aConditions: 0.1 M borate, pH 9.0; temperature = 20 °C. All kinetic parameters represent an average from at least three independent experiments with the uncertainty representing \pm sem from the nonlinear fits to the data. ^{bD} $k_{cat} = k_{cat}(H)/k_{cat}(D)$. ^c $\Delta E_a = E_a(D) - E_a(H)$. ^dKinetic parameters from ref 26. ^eKinetic parameters from ref 25.

ature dependencies of the first-order reaction rates (i.e., activation energy, $E_{\rm a}$) originate, at least in part, from the conformational reorganization of the ES complex to (i) reduce the donor—acceptor distance, (ii) align the active site geometries, and (iii) provide the proper electrostatics necessary to achieve effective wave function overlap. Thus, the change in the $E_{\rm a}$ from GLN MoLOX likely originates from a structural/dynamical impact to the protein.

Impact on MoLOX Substrate Specificity. Steady-state kinetics of WT MoLOX and variants were determined by measuring and comparing the first-order (k_{cat}) and secondorder $(k_{cat}/K_{\rm M})$ rate constants for the reactions involving different substrates; these values were then compared to the reaction with LA. The other substrates chosen were α linolenic (αLA) and γ linolenic acid (γLA) as well as a nonphysiological substrate, arachidonic acid (AA). Based on the first-order rate constants, WT MoLOX reacts nearly twice as fast with α LA as with LA, with the following order of reaction rates listed in decreasing rate: α LA, LA, AA, and γ LA. All MoLOX variants showed similar trends in the $k_{\rm cat}$ values for this panel of substrates (Table S2). Notably, the GLN variant showed elevated first-order rate constants for each of the substrates, relative to those for WT MoLOX. The corresponding ratio of k_{cat} values for each of the substrates, relative to the k_{cat} for LA, was invariant across the MoLOX variants (Figure 3A and Table S2).

GLN MoLOX showed an increased second-order rate constant for LA, relative to WT MoLOX. The effects of deglycosylation on $k_{\rm cat}/{\rm K_M}$ values were dependent upon the substrate tested (Table S2). The analysis of the ratio of $k_{\rm cat}/{\rm K_M}$ values relative to that for LA (i.e., $(k_{\rm cat}/{\rm K_M})^{\rm x}/(k_{\rm cat}/{\rm K_M})^{\rm LA})$, ENDO, and PNG variants showed similar effects with an increase for α LA and AA (not available in plants) over the LA substrate, whereas the proficiency of γ LA oxidation nearly matched LA (Table S3 and Figure 3B). Conversely, the GLN variant showed an increased preference toward LA, with all $(k_{\rm cat}/{\rm K_M})^{\rm x}/(k_{\rm cat}/{\rm K_M})^{\rm LA}$ ratios less than 1. Thus, the substitution of Asn-to-Gln had the greatest impact on substrate selectivity.

Analysis of Enzyme–Substrate (ES) Complex of *Mo*LOX Using ENDOR Spectroscopy. To build a structural basis for understanding the impact of surface glycan alteration on the structure of the *Mo*LOX-LA complex, herein, we employed ¹³C electron–nuclear double resonance (ENDOR) spectroscopy. We previously reported the ENDOR-derived active site structure of fully glycosylated WT *Mo*LOX-LA ES complex (Figure 4A).²⁵ The distances of C-11 and C-10 nuclei of selectively ¹³C labeled LA from the manganese (Mn²⁺) metallocenter at the LOX active site were obtained by measuring the electron–nuclear hyperfine coupling tensor (A) between the protein-bound Mn²⁺ and ¹³C10/¹³C11 nuclei of substrate. Since LA is not directly coordinated with Mn²⁺, A



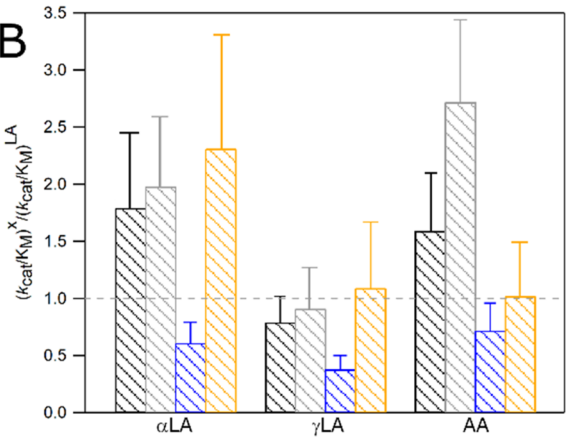


Figure 3. Comparative (A) first- and (B) second-order rate constants for the reaction of *Mo*LOX with various substrates. The color coding corresponds to the following: black, WT; gray, ENDO; blue, GLN; orange, PNG *Mo*LOX variants. Kinetics were collected noncompetitively at 20 °C in 0.1 M borate, pH 9.0 buffer. Refer to Tables S2 and S3 for tabulated kinetic parameters.

is purely dependent on the distances of Mn–C10/C11 (i.e., $r_{\rm Mn-C10}$, $r_{\rm Mn-C11}$) so the measurements with the ¹³C11 LA directly give $r_{\rm Mn-C11}$, the distance between Mn and the target substrate carbon (eq 2 of ref 25) (Figure 4A). Further, analysis of ¹³C, ¹H ENDOR spectra recorded at several magnetic fields across the EPR spectral envelope for ¹³C10 and ¹³C11 LA provides the relative orientation between the C10–C11 fragment of LA, Mn–H₂O, and the water proton, Mn–¹H. The C11–Mn and C10–Mn distances are then used as corresponding restraints in molecular dynamics (MD) simulations that can determine the hydrogen donor and acceptor (Mn-bound oxygen) distance, DAD, in the ground state (Figure 4A).

The zero-field splitting of the S = 5/2 Mn²⁺ EPR spectra reports on the symmetry of the first coordination sphere

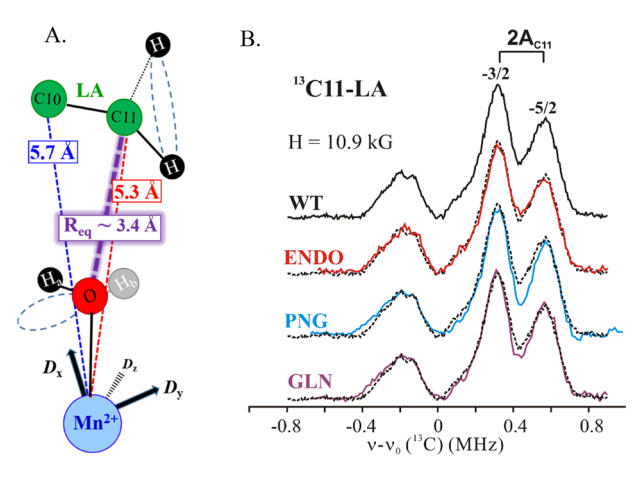


Figure 4. (A) ENDOR-derived ES ground-state structure of active site of LA in WT MoLOX. ²⁵ (B) 35 GHz ¹³C Mims ENDOR of WT MoLOX with ¹³C11-LA WT (black) and ENDO (red); ²⁵ PNG (cyan) and GLN (purple) here recorded at magnetic field H=10.9 kG. WT spectrum (dotted lines) is overlaid with each of the other MoLOX variants. Experimental conditions: MW frequency, ~34.8 GHz; MW pulse length ($\pi/2$), 50 ns; τ , 1500 ns; RF pulse length, 20 μ s; repetition rate,100 Hz; temperature, 2 K. The labels -5/2, -3/2 represent the ENDOR transitions that correspond to electron spin transition levels -5/2, -3/2. ²⁵ Panel A is reproduced from ref 25, published 2023 American Chemical Society.

surrounding Mn²⁺. The EPR spectra of WT *Mo*LOX and of the three glycan-altered variants, ENDO, PNG and GLN, are all superimposable, indicating that glycan alteration has no effect on the local structure of Mn-active site (Figure S2). To test the

consequence of surface modifications on the relative positioning of the substrate LA with respect to the Mn2+ center, we then analyzed and compared ENDOR data of WT enzyme and three different N-linked glycan modifications. The ¹³C10, ¹³C11 ENDOR spectra of the WT MoLOX with LA recorded at carefully selected magnetic fields across the EPR envelope overlay exceptionally well with those from ENDO, 25 PNG (Figure S3), and GLN (Figure S4). Correspondingly, as shown in Figure 4B, the ¹³C ENDOR spectra for labeled ¹³C11-LA at 10.9 kG, a magnetic field that provides the maximum resolution for ENDOR peaks, are fully superimposable on ¹³C ENDOR responses from the suite of glycosylation variants of MoLOX. The hyperfine coupling, A (direct readout from the ENDOR peaks), is unchanged by deglycosylation, and thus so are the Mn-C10 and Mn-C11 distances (as computed using eq 2²⁵). These data thus show that the removal or alteration of the glycans at the surface of MoLOX does not significantly influence the positioning of the substrate in the ground state ES complex.

HDX-MS properties of WT MoLOX. We next carried out HDX-MS to provide spatial resolution of the effect of deglycosylation on the protein structure and dynamics. HDX-MS reports on the regional changes in protein structure and flexibility as read out in altered deuterium exchange of the peptidyl backbone when native and "mutant" forms are compared. This technique has been used previously to characterize the alterations in regional protein dynamics as a result of modification of carbohydrates for select glycoproteins. 44–47

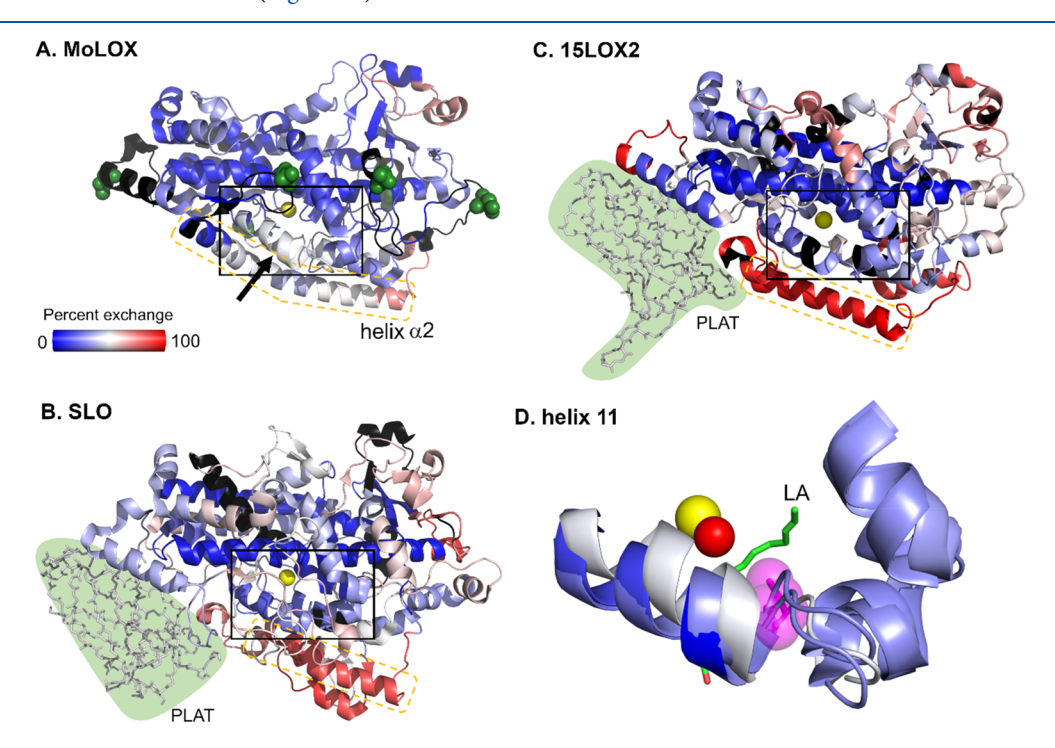


Figure 5. HDX-MS properties of fungal, plant, and animal LOX isozymes collected at 20 $^{\circ}$ C and 2 h (A–C). The catalytic metal is represented as a yellow sphere, and the Asn residues that form glycosidic bonds are shown as green spheres. The black arrow represents the putative substrate entrance portal. (B) and (C) show the comparative HDX-MS maps previously reported for the paradigmatic plant (SLO 30) and animal (15LOX2 49) lipoxygenases, respectively. The N-terminal "PLAT" (green shading) is a regulatory domain, not present in fungal LOXs. (D) The arched helix (helix 11) of the LOXs (as highlighted by box in parts A–C) is overlaid. The conserved leucine residue (L331 in *Mo*LOX; L546 in SLO; L420 in 15LOX2) that positions the substrate for C–H cleavage by the metal-hydroxide cofactor is represented by pink spheres for reference. Helix α2 for each LOX isozyme is outlined by dashed orange box.

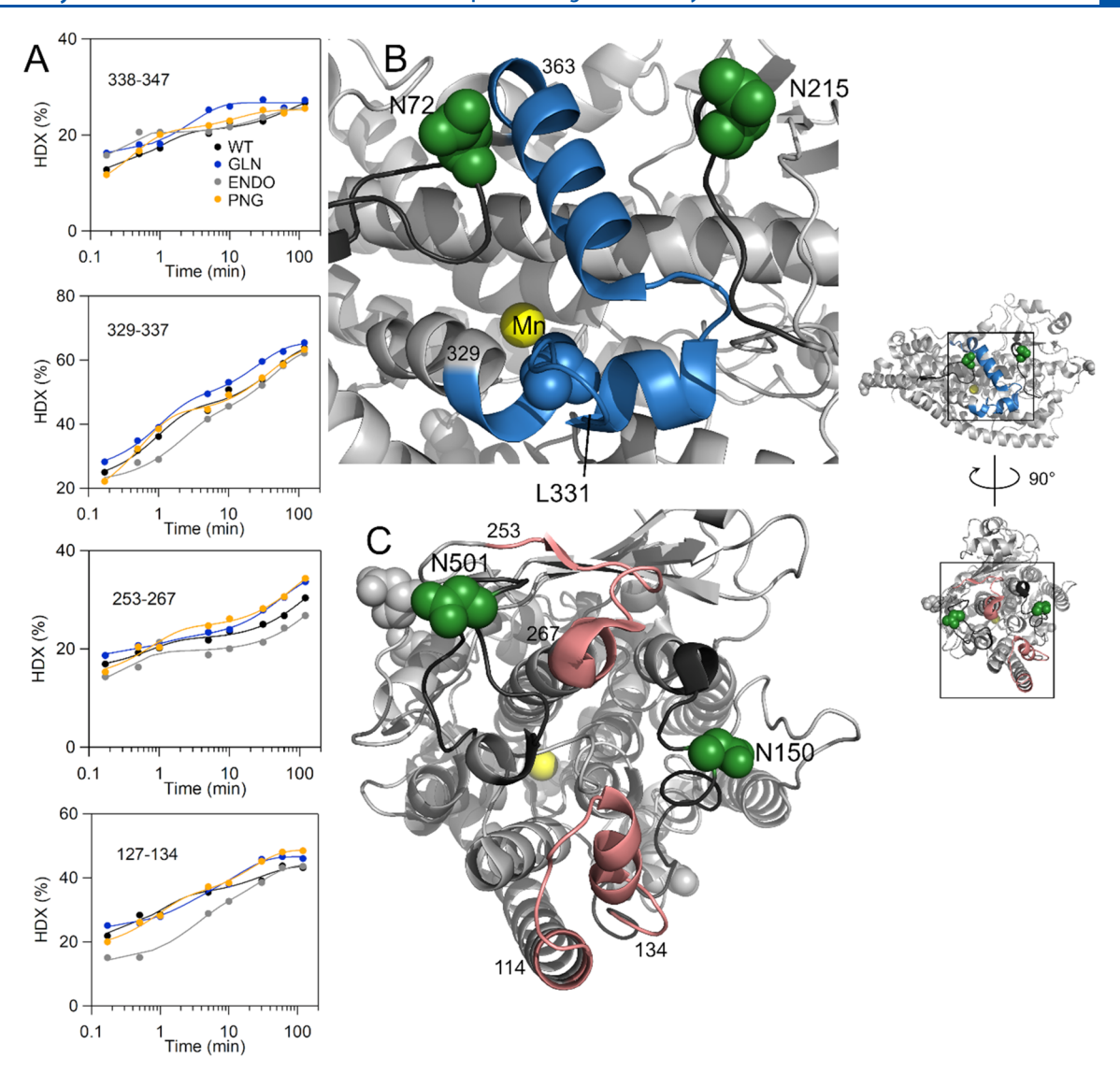


Figure 6. HDX-MS traces, collected at 20 °C, highlighting the differences between WT (black), ENDO (gray), PNG (gold), and GLN (blue) MoLOX (A). The locations of these effects are mapped onto the crystal structure of MoLOX (B, C). Note that panel C represents the protein structure from panel B, rotated 90°. The green spheres represent the Asn residues predicted to contain a glycosidic bond.

From the tandem MS data, ~350 total peptides of WT MoLOX were identified and assigned, corresponding to 82% coverage. From this list, we selected 33 reproducible, nonoverlapping peptides that cover 79% of the primary sequence for data reduction purposes. Note that the first 55 residues were not resolved in the coverage due to three sites of N-linked glycosylation (N18, N28, and N48) at the Nterminus. The assignment of peptides containing N-linked glycosylation sites in MoLOX was prevented by the heterogeneous nature of the glycans. The HDX-MS behavior of MoLOX in percent exchange at 2 h and 20 °C is mapped onto the structural model in Figure 5A. Overall, the exchange behavior in this catalytic domain is consistent with the expected patterns of the common LOX fold (see below) and tracks the trends in the X-ray derived B-factors determined from the EndoH-treated MoLOX structure (Figure S5).

In Figure 5, the HDX behavior of MoLOX is compared to two canonical iron LOXs, SLO (plant) and human 15LOX2 (animal). There are two notable differences in the exchange behavior for MoLOX. First is the exchange behavior at helix $\alpha 2$. Both the extent and rate of exchange for helix $\alpha 2$ in

MoLOX is dramatically reduced relative to both SLO and 15LOX2 (Figure 5A–C; box outline). This behavior supports a rigidification or structuring of helix α 2 for MoLOX. The distinct hydrogen exchange behavior for helix α 2 of MoLOX is likely to be due to the unique structural property of this helix, relative to that of SLO and 15LOX2. In SLO and 15LOX2, helix α 2 covers and gates the entrance to the substrate portal. From comparisons of the X-ray structures (Figure 5A–C), the architecture of helix $\alpha 2$ in MoLOX is quite distinct from the plant and animal representatives, forming a long, bent-like, but contiguous helix. The helix $\alpha 2$ structures of plant and animal LOXs display 3-6 helical turns. Conversely, this helix in MoLOX extends over 11 turns and traverses nearly the entire length of the catalytic domain. Further, unlike the canonical iron LOXs from plants and animals, the entrance to the substrate portal is open in MoLOX (Figure S6).

Second is the elevated H/D exchange of helix 11 (also referred to as the arched helix) in MoLOX that indicates a higher degree of flexibility compared to its plant and animal homologues (Figure 5D). The arched helix is disrupted by an unstructured loop (residues 331–336 in MoLOX) located in

the central part of the helix. In agreement with our HDX data, comparative crystal structures of a fungal LOX from F. graminearum revealed variable conformations of the arched helix that is suggestive of a high degree of flexibility, which is not seen in iron LOXs. 48

HDX-MS of MoLOX Variants Reveals Localized Altered Protein Flexibility. HDX-MS experiments were further performed on the ENDO, PNG, and GLN variants of MoLOX to determine changes in the regional conformational flexibility stemming from changes in glycosylation. From the analysis of the 33 nonoverlapping peptides, we identified two regions with differing exchange behavior for this suite of MoLOX variants (Figure 6). The first region includes a set of two peptides (residues 329-337 and 338-347), in which the GLN variant (Figure 6A, blue traces) exhibits a significant increase in exchange percentage ($\Delta HDX \geq 4\%$) at longer incubation times (≥3 min) relative to WT MoLOX (Figure 6A, black traces). These exchange properties correspond to enhanced protein flexibility for this variant. The peptides do not contain a glycosylation site but are flanked by two N-linked glycosylation sites, N72 and N215. The HDX pattern emerging for GLN MoLOX is potentially significant to catalysis as helix 11 (the arched helix) is positioned over the face of the catalytic center and contains the invariant and catalytically important Leu331. This leucine residue is considered to play an important role in substrate positioning and catalysis in LOXs.^{2,50}

A second region of protein was also impacted, including residues 114-134 and 253-267. The same trends are also shown in these regions with ENDO causing a reduced extent of exchange and the GLN variant linked to a slight increase in the extent of exchange. However, given that the latter peptides are ≥ 24 Å from the catalytic metal, it is unlikely that these altered peptide flexibilities lead to the impacted catalytic properties reported in Table 1 and Figure 3.

Single N-Linked Glycan Sequon Knockout MoLOX Variants. Based on the results emerging from HDX-MS, we predicted that the dramatic effects of deglycosylation on active site proficiency were likely originating from the removal of Nlinked glycan sequon(s) proximal to the arched helix, including N72 and N215. To provide support for this prediction, residues Asn72 and Asn215 were each singly converted to glutamine (i.e., N72Q and N215Q) and expressed and isolated from yeast cultures, as described above. The thermal and proteolytic stability were comparable to that seen for WT MoLOX (see Figure 2 and Table S1). The steady-state kinetic studies (Table S2) show modest increases in k_{cat} for the single glycan knockouts, relative to WT. As shown in Figure 7, the N72Q single mutant showed an increase in the second-order rate constant, $k_{\rm cat}/K_{\rm M}$, for LA (0.34 \pm 0.07 $\mu{\rm M}^{-1}$ s⁻¹) compared to WT (0.17 \pm 0.03 $\mu{\rm M}^{-1}$ s⁻¹) and matches the level of the GLN variant (0.34 \pm 0.08 μ M⁻¹ s⁻¹). Conversely, the N215Q single mutation showed only a slight increase in the second-order rate constant $(0.24 \pm 0.06 \,\mu\text{M}^{-1}\,\text{s}^{-1})$ relative to WT. Steady-state analysis was extended to the same panel of fatty acid substrates and compared to these second-order rate constants for LA reactions to assess the impact on substrate selectivity. Overall, the comparative second-order rate constants of N72Q were seen to track the GLN variant for both α LA/LA and γ LA/LA while the same ratios for the N215Q variant closely resembled those observed for WT MoLOX (Figure 7 and Table S5).

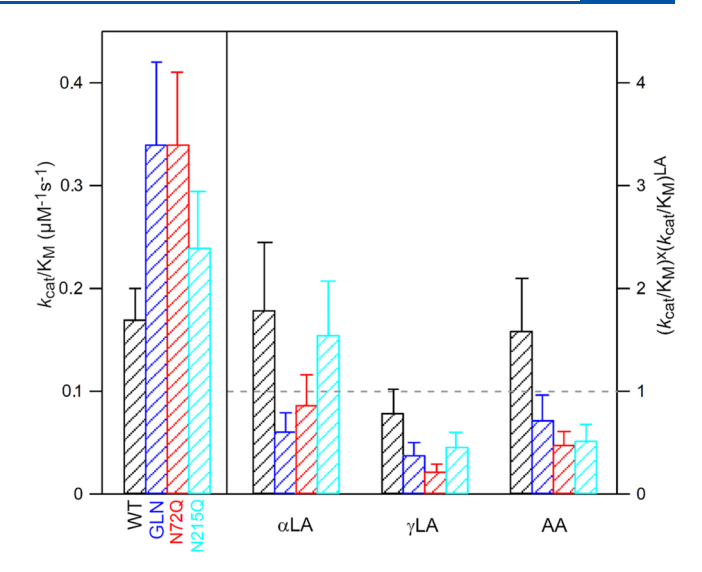


Figure 7. Enzyme proficiency and substrate specificity for WT *Mo*LOX and the Asn-to-Gln mutations. The colors correspond to the following: black, WT; blue, GLN; red, N72Q; cyan, N215Q.

Both enzyme single mutants exhibited AA/LA substrate selectivity ratios different than GLN or WT MoLOX. This kinetic property suggests that the link between substrate capture and glycosylation state is complex and likely not controlled by a single glycosylation site. These cumulative kinetic data for the single mutations provide strong support for the role of N-linked glycosylation site(s) adjacent to the active site in influencing local protein structure/dynamics that translates to altered enzymatic properties. Our results align with previously reported altered kinetic effects in other glycoenzymes stemming from single glycan sequon knockouts. ^{23,24,51,52}

DISCUSSION

In this study, we present the effects of N-linked glycosylation on the function and protein structure and dynamics of MoLOX, a representative fungal lipoxygenase. These PTMs are a common feature among the fungal LOXs that differentiates them from the canonical plant and animal enzymes. Kinetic and structural differences reported herein were most notable for a deglycosylated form of MoLOX, "GLN", that was generated through the mutation of the asparagine residues of eight predicted sites of N-linked glycans to glutamine (Figure 1). First is a change in the activation energy (E_a) for the reaction of MoLOX with LA. The second is the change in the relative catalytic proficiencies of the enzyme reaction, when LA, α LA, and γ LA are compared.

For the MoLOX reaction with LA, there was little impact on the kinetic isotope effect, $^Dk_{cat}$, and its temperature dependence $(\Delta E_a = E_a(\mathrm{H}) - E_a(\mathrm{D}))$, when WT and deglycosylated variants were compared (Table 1). In these tunneling reactions, ΔE_a has emerged as a kinetic ruler for tunneling efficiency. Small, near-zero values of ΔE_a serve as a litmus test of nonclassical hydrogen tunneling in native enzymes, whereas increases in the ΔE_a that result from a perturbation to the system (e.g., as caused by a site-strategic mutation) indicate decreased effectiveness of wave function overlap. The unchanged kinetic isotope effect parameters across the MoLOX variants suggest that the tunneling efficiency was largely unaffected by removal of surface glycans from the protein. This

result is further consistent with the ENDOR results on the structure of the ground-state MoLOX-LA complex. The ENDOR spectra for enzyme prepared by each of the degylcosylation methods nearly overlap the ENDOR spectra for the WT MoLOX variant. Note that the ENDOR data reports on the ground-state ES complex. The loss of surface glycans by asparagine-to-glutamine mutagenesis thus does not perturb the ground-state ES structure at the active site. In contrast, the kinetic isotope effect parameters (i.e., $^Dk_{\rm cat}$ and $\Delta E_{\rm a}$) report on the efficiency of wave function overlap at the tunneling-ready state of the enzyme reaction. The combined results from the kinetic measurements including kinetic isotope effects and ENDOR spectroscopy therefore provide complementary information about the precision of substrate positioning in the active site.

Localized Altered Protein Flexibility of MoLOX by Deglycosylation Detected by HDX. HDX analysis detected a notable increased flexibility to peptides contained within helix 11 (arched helix) for the GLN MoLOX variant over the WT, glycosylated protein (Figure 5). The arched helix covers the active site substrate channel and contains a strictly conserved leucine (L331 in MoLOX) that is important in positioning the substrate with respect to the metallocofactor.²⁵ Adjacent to L331 and the disrupted loop of the arched helix is a bulky phenylalanine residue at position 332. The mutation of Phe332 to volume-reducing alanine was associated with a decrease in the E_a from ~10 kcal/mol in WT to 7 kcal/mol for F332A.²⁵ Because the E_a for the rate-limiting H-transfer reaction is related to protein thermal motions, this result thus shows that the dynamics of the arched helix (helix 11) influence MoLOX catalysis and suggests that enhanced flexibility of the arched helix within the GLN variant may explain its increased activation energy, $E_{\rm a}$, for reaction with LA (Table 1).

Increased structural flexibility as glycans are removed from the MoLOX aligns with the expectations from previous computational modeling studies of various glycoproteins. 15,53 Protein structures and dynamics can be slaved to the solvent, 54 and the presence of glycans can interfere with the contacts between the solvent and the protein through steric shielding and can therefore convert the protein from solvent slaved to nonslaved.⁵³ Consistent with this hypothesis, previous solvent viscogen studies of MoLOX showed that the reaction with LA is viscosity independent and not slaved to the solvent. 55 This "decoupling" phenomena may also explain why there is no significant kinetic or structural effect stemming from the processing of MoLOX by endoglycosidase H. Endo H leaves a monosaccharide remaining at the protein surface. Since the solvent hydration layer at the protein surface is only a few water molecules thick, 56,57 reducing a complex carbohydrate to a monosaccharide might have a minimal-to-no impact on the solvent shielding.

Notably, the HDX behavior of the central region of helix $\alpha 2$, spanning residues 79–118, is virtually unchanged among the various glycan forms of MoLOX (Figure S7), despite a change in substrate selectivity for the GLN variant. This observation is in stark contrast to the patterns of regional flexibility that are responsive to activity-altering mutations in plant and animal LOXs. Specifically, the mutation to alanine of select large aliphatic residues lining the substrate entrance and binding channel in SLO increased off rates for substrate dissociation from the enzyme. HDX-MS analysis showed that increased mobility of helix $\alpha 2$, among a network of helices flanking the

active site, may be related to the enhanced commitment to catalysis in SLO. 43 Further, the structure and dynamics of helix $\alpha 2$ in SLO and human LOXs have also been shown to be responsive to substrates, inhibitors, and allosteric effectors. $^{3,31,49,59-61}$ Thus, from the extensive structural and kinetic studies of SLO and human LOXs, a generalized model is emerging that links helix $\alpha 2$ structure and dynamics to the regulation of substrate acquisition in plant and animal LOXs. 62 In contrast, based on the present kinetic and HDX-MS study, the mobility of helix $\alpha 2$ in MoLOX does not appear to be involved in regulation of enzyme reactivity and this enzyme is therefore functionally and structurally divergent from plant and animal LOXs.

Biochemical Role for N-Linked Glycosylation in Fungal LOXs. Perhaps the most significant impact on the structure of MoLOX stemming from loss of the N-linked glycosylation sites is the increased susceptibility of the protein to proteolysis by trypsin. Our limited-proteolysis experiment shows a significant trypsin degradation of GLN variant relative to WT MoLOX. However, both CD and HDX experiments support that the global protein structure is uncompromised upon deglycosylation. Together, these data indicate that glycans protect against proteases, which is expected to enhance the enzyme's biological function. Previous studies showed that the mRNA levels of MoLOX spike upon formation of the appressorium, a marker for the onset of rice infection.⁶³ Further, MoLOX is secreted by M. oryzae along with lipases to oxidize cell membrane lipids, leading to rice leaf necrosis, and thereby contributing to pathogenesis. 64 As a response to pathogen infection, protease expression is upregulated by plants as a part of their defense response. 65 The N-linked glycosylation of fungal LOXs, which are secreted during pathogenic attack, therefore provides an advantage for the fungal pathogen against the plant's defense mechanism.

Absence of Effect of PNGase on the Release of **MoLOX N-Glycans.** The lack of an effect of HDX at active site peptides for the PNG sample may be attributed to incomplete removal of glycans. Our SDS-PAGE analysis (Figure S1) shows that PNGaseF-treated MoLOX runs at an elevated migration of ~85-90 kDa, relative to ENDO MoLOX or the theoretical mass of deglycosylated MoLOX (67 kDa). The migration difference is consistent with 3-4 glycans remaining attached to the protein after processing with PNGase F. Previous MS/MS experiments on the PNG variant was only able to assign four (out of seven originally predicted) glycan sites (N18, N28, N48, and N501) by the presence of Asp at the predicted glycan sites. Among the glycan sites missing from this peptide assignment are the (N/D)72 and (N/D)215 residues, suggesting that these two sites are not processed by the PNGase F endoglycosidase. These two glycan sites are shown herein to modulate the dynamics of the arched helix that in turn influences catalytic properties (i.e., activation energy and substrate selectivity). Indeed, PNG MoLOX exhibited a nearly identical E_a for the reaction with LA, and a similar substrate selectivity profile to that of the WT enzyme. Further, the HDX properties of MoLOX, especially for peptides 329-337 and 338-347, are comparable for WT and PNG. We conclude that the lack of catalytic divergence from PNG MoLOX is likely attributed to incomplete deglycosylation, in particular at the two glycosylation sites (N72 and N215) that have the greatest influence on catalysis. Note that increasing the incubation temperature or PNG:Mo-LOX ratio did not change the efficiency of the reaction. Thus,

PNGase F appears to be unable to process all glycosylation sites on MoLOX, presumably due either to steric inaccessibility or the nature of the core structure of the glycan(s). For example, PNGase F cannot release glycans with core $\alpha(1,3)$ fucose attached.

We have further examined a PNGase from Rudaea cellulosilytica (PNGase Rc) that has recently been reported to exhibit improved activity, and tested whether it can overcome the limitations of current commercially available PNGase orthologues in processing at least this glycoprotein. In our hands, the MoLOX sample treated with PNGase Rc produced comparable processing to that of PNGase F, when the reaction pH was maintained at pH 5 (Figure S1). At pH values lower than F, where PNGase F activity is optimal (pH F 3.5), the deglycosylated MoLOX sample aggregated during the F 16–20 h reaction times required for complete processing. Thus, the PNGase F could not be used to produce the large quantities of the desired deglycosylated form of F 16–17 for structural and functional studies.

CONCLUSION

The current work presents the effect of glycan modifications on the structure-dynamics-function of the fungal lipoxygenase, MoLOX. Release of N-linked glycans by mutagenesis or the glycosidases Endo H and PNGase F had no effect on the local ground-state enzyme-substrate structures determined by ENDOR spectroscopy, and the hydrogen tunneling properties of catalysis were likewise unchanged. However, mutation of all N-linked glycosylation sequons by replacement of asparagine to glutamine resulted in an increased activation barrier, E_{a} , for hydrogen tunneling in the MoLOX reaction. The elevated E_a from this GLN variant implies an impact on the protein dynamics related to catalysis. This effect was accompanied by an increased susceptibility of the deglycosylated MoLOX forms to trypsin, indicating that the extensive glycosylation protects the native enzyme, secreted during pathogenesis, from degradation by plant proteases.

Correspondingly, HDX-MS analysis of the deglycosylated variants revealed a localized enhancement in flexibility for GLN MoLOX along the arched helix that blankets the binding channel of fatty acid substrates. This peptide region does not contain a glycosylation sequon but is flanked by two loops that each contain a glycosylation site, N72 and N215. Removal of one or both glycans was predicted to influence catalysis at the active site through altered dynamics of the arched helix. The functional effects stemming from these select N-linked glycans were validated through site-selective knockouts, with the largest effect at position 72, in which N72Q exhibits nearly identical catalytic properties to the fully deglycosylated GLN MoLOX variant. The observation of subtle, local changes in HDX at the arched helix contrasts with the emerging model that links helix α 2 structure and dynamics to the regulation of substrate acquisition in plant and animal LOXs.^{3,62} Instead, HDX-MS studies suggest the mobility of helix α 2 does not appear to play a role in regulation of MoLOX reactivity, and thus, in this way fungal LOXs are functionally and structurally divergent from plant and animal LOXs.

ASSOCIATED CONTENT

Supporting Information

The Supporting Information is available free of charge at https://pubs.acs.org/doi/10.1021/acs.biochem.4c00109.

% HDX values using HDX WorkBench software (XLSX) SDS-PAGE and CD analysis of MoLOX variants; EPR and complete 2D ^{13}C ENDOR spectra of LA in MoLOX variants; HDX-MS analysis of helix $\alpha 2$; and enzyme kinetics (PDF)

Accession Codes

Protein Identifier MoLOX, Uniprot G4NAP4.

AUTHOR INFORMATION

Corresponding Author

Adam R. Offenbacher – Department of Chemistry, East Carolina University, Greenville, North Carolina 27858, United States; Occid.org/0000-0001-6990-7178; Email: offenbachera17@ecu.edu

Authors

Chris Whittington — Department of Chemistry, East Carolina University, Greenville, North Carolina 27858, United States; Present Address: Department of Chemistry and Biochemistry, Georgia Institute of Technology, Atlanta, GA, United States

Ajay Sharma — Department of Chemistry, Northwestern University, Evanston, Illinois 60208, United States; orcid.org/0000-0002-0829-6753

S. Gage Hill – Department of Chemistry, East Carolina University, Greenville, North Carolina 27858, United States; orcid.org/0000-0002-0650-2293

Anthony T. Iavarone — California Institute for Quantitative Biosciences, Department of Chemistry, University of California, Berkeley, Berkeley, California 94720, United States

Brian M. Hoffman — Department of Chemistry, Northwestern University, Evanston, Illinois 60208, United States; orcid.org/0000-0002-3100-0746

Complete contact information is available at: https://pubs.acs.org/10.1021/acs.biochem.4c00109

Funding

This work was supported by the National Institutes of Health (Grant R01GM111097) to B.M.H. and the National Science Foundation (Grant 22-31079) to A.R.O.

Notes

The authors declare no competing financial interest.

ACKNOWLEDGMENTS

We thank Prof. Anne Zeck from the University of Tuebingen for the generous gift of the expression vector for PNGase Rc.

REFERENCES

- (1) Liavonchanka, A.; Feussner, I. Lipoxygenases: occurrence, functions and catalysis. *J. Plant Phys.* **2006**, *163*, 348–357.
- (2) Newcomer, M. E.; Brash, A. R. The structural basis for specificity in lipoxygenase catalysis. *Protein Sci.* **2015**, *24*, 298–309.
- (3) Offenbacher, A. R.; Holman, T. R. Fatty acid allosteric regulation of C-H activation in plant and animal lipoxygenases. *Molecules* **2020**, 25, 3374.
- (4) Hornsten, L.; Su, C.; Osbourn, A. E.; Hellman, U.; Oliw, E. H. Cloning of the manganese lipoxygenase gene reveals homology with the lipoxygenase gene family. *Eur. J. Biochem.* **2002**, *269*, *2690*–*2697*.
- (5) Brodhun, F.; Cristobal-Sarramian, A.; Zabel, S.; Newie, J.; Hamberg, M.; Feussner, I. An iron 13S-lipoxygenase with an alphalinolenic acid specific hydroperoxidase activity from *Fusarium oxysporum*. *PLoS One* **2013**, *8*, No. e64919.

- (6) Wennman, A.; Jerneren, F.; Magnuson, A.; Oliw, E. H. Expression and characterization of manganese lipoxygenase of the rice blast fungus reveals prominent sequential lipoxygenation of α -linolenic acid. *Arch. Biochem. Biophys.* **2015**, 583, 87–95.
- (7) Oliw, E. H. Diversity of the manganese lipoxygenase gene family. *Fungal Genet. Biol.* **2022**, *163*, 103746.
- (8) Soanes, D. M.; Chakrabarti, A.; Paszkiewicz, K. H.; Dawe, A. L.; Talbot, N. J. Genome-wide transcriptional profiling of appressorium development by the rice blast fungus *Magnaporthe oryzae*. *PLoS Pathog.* **2012**, *8*, No. e1002514.
- (9) Su, C.; Oliw, E. H. Manganese lipoxygenase. Purification and characterization. *J. Biol. Chem.* **1998**, 273, 13072–13079.
- (10) Cristea, M.; Engström, Å.; Su, C.; Hörnsten, L.; Oliw, E. H. Expression of manganese lipoxygenase in Pichia pastoris and site-directed mutagenesis of putative metal ligands. *Arch. Biochem. Biophys.* **2005**, 434, 201–211.
- (11) Dwek, R. A. Glycobiology: toward understanding the function of sugars. *Chem. Rev.* **1996**, *96*, 683–720.
- (12) Flynn, R. A.; Pedram, K.; Malaker, S.; Batista, P. J.; Smith, B. A. H.; Johnson, A. G.; George, B. M.; Majzoub, K.; Villalta, P. W.; Carette, J. E.; Bertozzi, C. R. Small RNAs are modified with N-glycans and displayed on the surface of living cells. *Cell* **2021**, *184*, 3109–3124.
- (13) Rudd, P. M.; Elliott, T.; Cresswell, P.; Wilson, I. A.; Dwek, R. A. Glycosylation and the immune system. *Science* **2001**, *291*, 2370–2376
- (14) Helenius, A.; Aebi, M. Roles of N-linked glycans in the endoplasmic reticulum. *Annu. Rev. Biochem.* **2004**, 73, 1019–1049.
- (15) Lee, H. S.; Qi, Y.; Im, W. Effects of N-glycosylation on protein conformation and dynamics: protein data bank analysis and molecular dynamics simulation. *Sci. Rep.* **2015**, *5*, 8926.
- (16) Ohtsubo, K.; Marth, J. D. Glycosylation in cellular mechanisms of health and disease. *Cell* **2006**, *126*, 855–867.
- (17) Ng, B. G.; Freeze, H. H. Perspectives on glycosylation and its congenital disorders. *Trends Genet.* **2018**, *34*, 466–476.
- (18) Reily, C.; Stewart, T. J.; Renfrow, M. B.; Novak, J. Glycosylation in health and disease. *Nat. Rev. Nephrol.* **2019**, *15*, 346–366.
- (19) Pinelo, J. E. E.; Manandhar, P.; Popovic, G.; Ray, K.; Tasdelen, M. F.; Nguyen, Q.; Iavarone, A. T.; Offenbacher, A. R.; Hudson, N. E.; Sen, M. Systematic mapping of the conformational landscape and dynamism of soluble fibrinogen. *J. Thromb. Haemost.* **2023**, *21*, 1529–1543.
- (20) Mechref, Y.; Novotny, M. V. Structural investigations of glycoconjugates at high sensitivity. *Chem. Rev.* **2002**, *102*, 321–370.
- (21) Skamnioti, P.; Gurr, S. J. Against the grain. Safeguarding rice from rice blast disease. *Trends Biotechnol.* **2009**, *27*, 141–150.
- (22) Wennman, A.; Oliw, E. H.; Karkehabadi, S.; Chen, Y. Crystal structure of manganese lipoxygenase of the rice blast fungus *Magnaporthe oryzae. J. Biol. Chem.* **2016**, 291, 8130–8139.
- (23) Skropeta, D. The effect of individual N-glycans on enzyme activity. *Bioorgan. Med. Chem.* **2009**, *17*, 2645–2653.
- (24) Ressler, V. T.; Raines, R. T. Consequences of the endogenous *N*-glycosylation of human ribonuclease 1. *Biochemistry* **2019**, *58*, 987–996.
- (25) Sharma, A.; Whittington, C.; Jabed, M.; Hill, S. G.; Kostenko, A.; Yu, T.; Li, P.; Doan, P. E.; Hoffman, B. M.; Offenbacher, A. R. ¹³C electron nuclear double resonance spectroscopy-guided molecular dynamics computations reveals the structure of the active site enzyme-substrate complex of an active, *N*-linked glycosylated lipoxygenase. *Biochemistry* **2023**, *62*, 1531–1543.
- (26) Kostenko, A.; Ray, K.; Iavarone, A. T.; Offenbacher, A. R. Kinetic characterization of the C-H activation step for the lipoxygenase from the pathogenic fungus *Magnaporthe oryzae*: impact of N-linked glycosylation. *Biochemistry* **2019**, *58*, 3193–3203.
- (27) Gupta, R.; Jung, E.; Brunak, S. NetNGlyc. 1.0 Server.
- (28) Rickert, K.; Klinman, J. P. Nature of hydrogen transfer in soybean lipoxygenase-1: separation of primary and secondary isotope effects. *Biochemistry* **1999**, *38*, 12218–12228.

- (29) Horitani, M.; Offenbacher, A. R.; Carr, C. A. M.; Yu, T.; Hoeke, V.; Cutsail, G. E., III; Hammes-Schiffer, S.; Klinman, J. P.; Hoffman, B. M. ¹³C ENDOR spectroscopy of lipoxygenase-substrate complexes reveals the structural basis for C-H activation by tunneling. *J. Am. Chem. Soc.* **2017**, *139*, 1984–1997.
- (30) Offenbacher, A. R.; Hu, S.; Poss, E. M.; Carr, C. A. M.; Scouras, A. D.; Prigozhin, D. M.; Iavarone, A. T.; Palla, A.; Alber, T.; Fraser, J. S.; Klinman, J. P. Hydrogen-deuterium exchange of lipoxygenase uncovers a relationship between distal, solvent exposed protein motions and the thermal activation barrier for catalytic proton-coupled electron tunneling. *ACS Cent. Sci.* **2017**, *3*, 570–579.
- (31) Offenbacher, A. R.; Iavarone, A. T.; Klinman, J. P. Hydrogendeuterium exchange reveals long-range dynamical allostery in soybean lipoxygenase. *J. Biol. Chem.* **2018**, 293, 1138–1148.
- (32) Pascal, B. D.; Willis, S.; Lauer, J. L.; Landgraf, R. R.; West, G. M.; Marciano, D.; Novick, S.; Goswami, D.; Chalmers, M. J.; Griffin, P. R. HDX Workbench: software for the analysis of H/D exchange MS data. J. Am. Soc. Mass Spectrom. 2012, 23, 1512–1521.
- (33) Sola, R. J.; Griebenow, K. A. I. Effects of glycosylation on the stability of protein pharmaceuticals. *J. Pharm. Sci.* **2009**, *98*, 1223–1245.
- (34) Yasumatsu, K.; Moritaka, S. Fatty acid compositions of rice lipid and their changes during storage. *Agr. Biol. Chem.* **1964**, 28, 257–264.
- (35) Hatcher, E.; Soudackov, A. V.; Hammes-Schiffer, S. Proton-coupled electron transfer in soybean lipoxygenase. *J. Am. Chem. Soc.* **2004**, 126, 5763–5775.
- (36) Klinman, J. P. Importance of protein dynamics during enzymatic C-H bond cleavage catalysis. *Biochemistry* **2013**, *52*, 2068–2077.
- (37) Klinman, J. P. A new model for the origin of kinetic hydrogen isotope effects. *J. Phys. Org. Chem.* **2010**, 23, 606–612.
- (38) Klinman, J. P.; Offenbacher, A. R. Understanding biological hydrogen transfer through the lens of temperature dependent kinetic isotope effects. *Acc. Chem. Res.* **2018**, *51*, 1966–1974.
- (39) Singh, P.; Vandemeulebroucke, A.; Li, J.; Schulenburg, C.; Fortunato, G.; Kohen, A.; Hilvert, D.; Cheatum, C. M. Evolution of the chemical step in enzyme catalysis. *ACS Catal.* **2021**, *11*, 6726–6732.
- (40) Kohen, A.; Jonsson, T.; Klinman, J. P. Effects of protein glycosylation on catalysis: changes in hydrogen tunneling and enthalpy of activation in the glucose oxidase reaction. *Biochemistry* **1997**, *36* (9), 2603–2611.
- (41) Soudackov, A. V.; Hammes-Schiffer, S. Proton-coupled electron transfer reactions: analytical rate constants and case study of kinetic isotope effects in lipoxygenase. *Faraday Disc.* **2016**, *195*, 171–189.
- (42) Klinman, J. P.; Offenbacher, A. R.; Hu, S. Origins of enzyme catalysis: experimental findings for C-H activation, new models and their relevance to prevailing theoretical constructs. *J. Am. Chem. Soc.* **2017**, *139*, 18409–18427.
- (43) Zaragoza, J. P. T.; Offenbacher, A. R.; Hu, S.; Gee, C. L.; Firestein, Z. M.; Minnetian, N.; Deng, Z.; Fan, F.; Iavarone, A. T.; Klinman, J. P. Temporal and spatial resolution of distal protein motions that activate hydrogen tunneling in soybean lipoxygenase. *Proc. Natl. Acad. Sci. U.S.A.* 2023, 120, No. e2211630120.
- (44) Houde, D.; Arndt, J.; Domeier, W.; Berkowitz, S.; Engen, J. R. Characterization of IgG1 conformation and conformational dynamics by hydrogen/deuterium exchange mass spectrometry. *Anal. Chem.* **2009**, *81*, 2644–2651.
- (45) Huang, R. Y. C.; Hudgens, J. W. Effects of desialylation on human α 1-acid glycoprotein-ligand interactions. *Biochemistry* **2013**, 52, 7127–7136.
- (46) Rose, R. J.; van Berkel, P. H. C.; van den Bremer, E. T. J.; Labrijn, A. F.; Vink, T.; Schuurman, J.; Heck, A. J. R.; Parren, P. W. H. I. Mutation of Y407 in the CH3 domain dramatically alters glycosylation and structure of human IgG. *mAbs* **2013**, *5*, 219–228.
- (47) Upton, R.; Migas, L. G.; Pacholarz, K. J.; Beniston, R. G.; Estdale, S.; Firth, D.; Barran, P. E. Hybrid mass spectrometry methods reveal lot-to-lot differences and delineate the effects of glycosylation

- on the tertiary structure of Herceptin(R). Chem. Sci. 2019, 10, 2811–2820.
- (48) Oliw, E. H. Thirty years with three-dimensional structures of lipoxygenases. *Arch. Biochem. Biophys.* **2024**, 752, 109874.
- (49) Tsai, W.-C.; Gilbert, N. C.; Ohler, A.; Armstrong, M.; Perry, S.; Kalyanaraman, C.; Yasgar, A.; Rai, G.; Simeonov, A.; Jadhav, A.; Standley, M.; Lee, H.-W.; Crews, P.; Iavarone, A. T.; Jacobson, M. P.; Neau, D. B.; Offenbacher, A. R.; Newcomer, M. E.; Holman, T. R. Kinetic and structural investigations of novel inhibitors of human epithelial 15-lipoxygenase-2. *Bioorgan. Med. Chem.* **2021**, *46*, 116349.
- (50) Hu, S.; Offenbacher, A. R.; Lu, E. D.; Klinman, J. P. Comparative kinetic isotope effects on first- and second-order rate constants of soybean lipoxygenase variants uncover a substrate-binding network. *J. Biol. Chem.* **2019**, *294*, 18069–18076.
- (51) Nuylert, A.; Ishida, Y.; Asano, Y. Effect of glycosylation on the biocatalytic properties of hydroxynitrile lyase from the passion fruit, Passiflora edulis: a comparison of natural and recombinant enzymes. *ChemBioChem* **2017**, *18* (3), 257–265.
- (52) Komaru, K.; Satou, Y.; Al-Shawafi, H. A.; Numa-Kinjoh, N.; Sohda, M.; Oda, K. Glycosylation-deficient mutations in tissue-nonspecific alkaline phosphatase impair its structure and function and are linked to infantile hypophosphatasia. *FEBS J.* **2016**, 283, 1168–1179.
- (53) Sola, R. J.; Rodriguez-Martinez, J. A.; Griebenow, K. A. I. Modulation of protein biophysical properties by chemical glycosylation: biochemical insights and biomedical implications. *Cell. Mol. Life Sci.* **2007**, *64*, 2133–2152.
- (54) Fenimore, P. W.; Frauenfelder, H.; McMahon, B. H.; Parak, F. G. Slaving: solvent fluctuations dominate protein dynamics and functions. *Proc. Natl. Acad. Sci. U.S.A.* **2002**, *99*, 16047–16051.
- (55) Guevara, L.; Gouge, M.; Ohler, A.; Hill, S. G.; Patel, S.; Offenbacher, A. R. Effect of solvent viscosity on the activation barrier of hydrogen tunneling in the lipoxygenase reaction. *Arch. Biochem. Biophys.* **2023**, 747, 109740.
- (56) Nandi, N.; Bagchi, B. Dielectric relaxation of biological water. J. Phys. Chem. B 1997, 101, 10954–10961.
- (57) Fenimore, P. W.; Frauenfelder, H.; McMahon, B. H.; Young, R. D. Bulk-solvent and hydration-shell fluctuations, similar to α and β -fluctuations in glasses, control protein motions and function. *Proc. Natl. Acad. Sci. U.S.A.* **2004**, *101*, 14408–14413.
- (58) Tran, M.; Signorelli, R. L.; Yamaguchi, A.; Chen, E.; Holinstat, M.; Iavarone, A. T.; Offenbacher, A. R.; Holman, T. Biochemical and hydrogen-deuterium exchange studies of the single nucleotide polymorphism Y649C in human platelet 12-lipoxygenase linked to a bleeding disorder. *Arch. Biochem. Biophys.* 2023, 733, 109472.
- (59) Bradshaw, M. D.; Gaffney, B. J. Fluctuations of an exposed pihelix involved in lipoxygenase substrate acquisition. *Biochemistry* **2014**, *53*, 5102–5110.
- (60) Droege, K. D.; Keithly, M. E.; Sanders, C. R.; Armstrong, R. N.; Thompson, M. K. Structural dynamics of 15-lipoxygenase-2 via hydrogen—deuterium exchange. *Biochemistry* **2017**, *56*, 5065–5074.
- (61) Mogul, R.; Johansen, E.; Holman, T. R. Oleyl sulfate reveals allosteric inhibition of soybean lipoxygenase-1 and human 15-lipoxygenase. *Biochemistry* **2000**, *39*, 4801–4807.
- (62) Gallegos, E. M.; Reed, T. D.; Mathes, F. A.; Guevara, N.; Neau, D.; Huang, W.; Newcomer, M. E.; Gilbert, N. C. Helical remodeling augments 5-lipoxygenase activity. *J. Biol. Chem.* **2022**, 298, 102282.
- (63) Soanes, D. M.; Chakrabarti, A.; Paszkiewicz, K. H.; Dawe, A. L.; Talbot, N. J. Genome-wide transcriptional profiling of appressorium development by the rice blast fungus *Magnaporthe oryzae*. *PLoS Pathog.* **2012**, *8*, No. e1002514.
- (64) Oliw, E. H. Iron and manganese lipoxygenase of plant pathogenic fungi and their role in biosynthesis of jasmonates. *Arch. Biochem. Biophys.* **2022**, 722, 109169.
- (65) Thomas, E. L.; van der Hoorn, R. A. L. Ten prominent host proteases in plant-pathogen interactions. *Int. J. Mol. Sci.* **2018**, *19*, 639.
- (66) Wang, T.; Voglmeir, J. PNGases as valuable tools in glycoprotein analysis. *Protein and Peptide Letters* **2014**, 21 (10), 976–985.

- (67) Tretter, V.; Altmann, F.; Marz, L. Peptide-N4-(N-acetyl- β -glucosaminyl) asparagine amidase F cannot release glycans with fucose attached α 1 → 3 to the asparagine-linked N-acetylglucosamine residue. *Eur. J. Biochem.* **1991**, *199*, 647–652.
- (68) Gramlich, M.; Maier, S.; Kaiser, P. D.; Traenkle, B.; Wagner, T. R.; Voglmeir, J.; Stoll, D.; Rothbauer, U.; Zeck, A. A novel PNGase Rc for improved protein *N*-deglycosylation in bioanalytics and hydrogen—deuterium exchange coupled with mass spectrometry epitope mapping under challenging conditions. *Anal. Chem.* **2022**, *94*, 9863—9871.